ACS APPLIED MATERIALS & INTERFACES

Research Article

www.acsami.org

(211)-Orientation Preference of Transparent Conducting In_2O_3:Sn Films and Its Formation Mechanism

Dongyun Wan,[†] Ping Chen,[†] Jun Liang,*[,†] Shaotang Li,[†] and Fuqiang Huang*[,†,‡]

[†]State Key Laboratory of High Performance Ceramics and Superfine Microstructure and CAS Key Laboratory of Materials for Energy Conversion, Shanghai Institute of Ceramics, Chinese Academy of Sciences, Shanghai 200050, China,

[‡]College of Chemistry & College of Engineering, Peking University, Beijing 100871, China

Supporting Information

ABSTRACT: Dominantly (211)-oriented In_2O_3:Sn (ITO) transparent conducting oxide (TCO) films were first fabricated at high sputtering power in the weak reducing ambient with superior electrical and optical properties. The dependence of ITO film orientation on growth condition was systematically investigated, and the formation mechanism was studied by surface energy calculation and band structure simulation. The unique properties of the (211)-oriented films should be ascribed to the richest In-terminated surface of the (211) plane, which is tightly correlated with the comparably highest surface energy and highest conduction band surface comparing with the other two typical planes of (222) and (400). The as-prepared (211)-oriented ITO films with the In-rich ending atoms on the surface are of great significance for the transparent electrode applications.

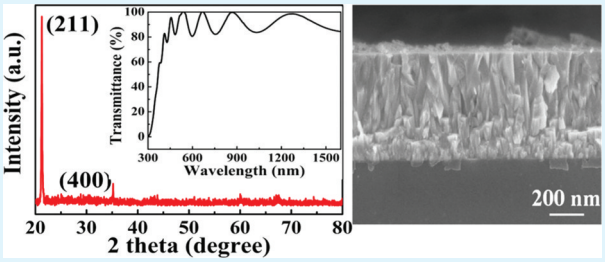

KEYWORDS: *In_2O_3:Sn thin films, (211)-oriented, transparent conducting oxide, surface modification, thin film solar cells*

1. INTRODUCTION

As a front electrode in thin film solar cells, transparent conductive oxide (TCO) films play a major role in determining the maximum attainable conversion efficiency.[1] In_2O_3:Sn (ITO) with unique electrical and optical properties[2−5] is one of the most popular TCO films. Their surface modification is important for energy conversion devices to improve electron transfer and further enhance device performance,[6−8] because different exposed facets in these polycrystalline films possess different arrangements of atoms to result in different chemistry and working function.

TCO films as a transparent electrode of devices, the ending atoms on the surface of films rule the interface of heterojunctions. For the thin film solar cells, the p-type solar absorber materials are nonoxides (Si, GaAs, $CuInSe_2$, CdTe, etc.), and so do the n-type materials (Si, GaN, ZnS, CdS). For the sake of charge transfer, the ending atoms of In atoms in ITO films are highly appreciated due to the highly dispersed In 5s conduction band, which causes the Moss-Burstein effect to result in the good conducting property of ITO. The ITO with a more In-ended surface has a better ability to transfer carriers, but the highly localized O^{2-} $2p^6$ states does not. Therefore, It is meaningful and significant to prepare the ITO film with a rich In-terminated surface to achieve a low interface electronic resistance.

In this paper, the dependence of ITO film orientation on growth condition was systematically investigated. The orientations of (222), (400), and (211) for ITO films were prepared by magnetron sputtering deposition method. Strongly (211)-oriented thin films were, for the first time, fabricated here at high sputtering power in the weak reducing atmosphere. Simulation shows that the surface dangling-bonds of In atoms for the (211) plane is much higher than that of (400) and (222) planes. The as-prepared (211) oriented film shows excellent wide-spectrum transparency (89.4% in 400−1100 nm) and electrical conductivity (R_s = 2.11 Ω/sq, $\rho = 1.03\times10^{-4}$ Ω cm). The superior properties of the (211) −oriented films should be attributed to the comparably highest surface energy and highest conduction band surface comparing with the other two planes of (222) and (400), which was verified by surface energy calculation and band structure simulation.

2. EXPERIMENTAL SECTION

The ITO films were deposited on glass slides in a JPG450 magnetron sputtering system equipped with a 3 in. magnetron gun (US'GUN). The RF power (13.56 MHz) was supplied by a generator (Advanced Energy) matched to the target through a tuning network. A ceramic In_2O_3:SnO_2 (90:10 wt %, 99.99% purity) was used as the target. An unthrottled base pressure of 2.0×10^{-4} Pa was reached using a combined vacuum system of mechanical pump and turbomolecular pump. All the experiments were conducted at nominally room temperature (the maximum temperature monitored being 55 °C) and under a flow of high-purity Ar gas (99.99%) or Ar/O_2 or Ar/H_2 mixture.

Ar/O_2 mixture (1-3% O_2 content), pure Argon (99.99%) and Ar/H_2 mixture (0.25-1.0% H_2 content) were utilized as working atmosphere at the certain sputtering power of 140 W to examine

Received: September 14, 2011
Accepted: November 21, 2011
Published: November 21, 2011

   dx.doi.org/10.1021/am2012432 | ACS Appl. Mater. Interfaces 2011, 3, 4751−4755

the effect of the atmosphere ambient on the change of the preferential orientation of the prepared ITO films. To examine the effect of different energy of impinging particles during the sputtering process on the change of the preferential orientation, two more experimental series were conducted under a flow of weak reduction ambient of Ar/H_2 mixture (0.5% H_2 content). The first one is the deposition of ITO layers with different working pressure (0.3-1.0 Pa) at a certain sputtering power of 140W, followed by a second series of the deposition of ITO layers with different sputtering power (100−160 W) at a certain working pressure of 0.3 Pa, the corresponding power densities varied from 2.19 to 3.51 W/cm^2 are in the range of the reported high values (1.27 − 6.29 W/cm^2).[9−11] Furthermore, unlike the reported high deposition temperature of 200−500 °C,[12−16] the sputtering in this study is conducted at room temperature without any external heating.

X-ray diffraction (XRD) measurements were carried out on a Bruker AXS D8 Advance Diffractometer using CuKα radiation to characterize the crystallization and phase structure of the films and target. Surface and cross-section morphologies of the ITO films were investigated by scanning electron microscopy (SEM, JOEL 6510), field emission scanning electron microscopy (FE-SEM, LEO-1530VP), and transmission electron microscopy (TEM, JEM2100F). A profilometer (Dektak 150) were used to evaluate the thickness of the ITO films. The van der Pauw method was used with an Accent HL5500 to measure the electrical transport properties including the resistivity, carrier concentration and Hall mobility. UV-visible-infrared transmission spectra of the films were recorded by a spectrophotometer (Hitachi UV-3010PC) between 300 and 2200 nm. The absorption spectra reported were obtained after subtracting the signal of the glass substrate.

3. RESULTS AND DISCUSSION

3.1. Preparation of Various Orientation Films. X-ray diffraction patterns of the ITO films are shown in Figure1. These films were deposited with Ar/O_2 mixture (1−3% O_2 content), pure Argon (99.99%) and Ar/H_2 mixture (0.25−1.0% H_2) working atmosphere at the certain sputtering power of 140 W and working pressure of 0.3 Pa. All the films have a single-phase diffraction pattern, which can be readily indexed to the cubic structure of In_2O_3 (JCPDS card no. 06-0416). The ITO films grown at an oxygen-contained atmosphere revealed a preferential crystallization along (222), and the 3% O_2/Ar film is more obviously preferential than the 1% O_2/Ar one. Contrarily, for the samples deposited in pure Argon, the (400) plane intensifies while the (222) diffraction peak disappears. At sufficient oxygen, stoichiometric In_2O_3 maintains and the crystal growth is preferentially with (222) plane. The (400) and (440) orientations appear if the film is sputtered with a high power in an oxygen deficient atmosphere. These results are consistent with the previously reported data.[6,17−23]

Different from any reported (222) or (400) oriented films, extremely strong (211) diffraction peaks were surprisingly observed in the weak reducing ambient containing 0.25-0.5% H_2, as shown in Figure 1. More significant orientation is for the 0.5% H_2 film than the 0.25% one. When further increasing the hydrogen content to 1.0% H_2, the preferential growth of (211) peak becomes weaker and the (400) diffraction peak increases again just like the film grown in pure Ar.

It seems that the weak reducing ambient favored or might play a critical role in forming the preferred orientation of the ITO grains along the (211) direction. To further test this hypothesis, we systematically studied the ITO films at different pressures and with different powers under a certain flow of weak reduction gas, as shown in Figure S1a & S1b (see the Supporting Information). It was demonstrated that the weak reducing ambient (0.25−0.5% H_2), high sputtering power (> 120 W), and low working pressure (< 0.5 Pa) are the required conditions to achieve the (211)-oriented films. The high working pressure (1.0 Pa) favors for the (222) preferential growth, and the (211) peak increases with the decrease of the working pressure. The low sputtering power favors for the (400) and (222) preferential growth, and the orientation switches to the (211) direction with increasing the sputtering power.

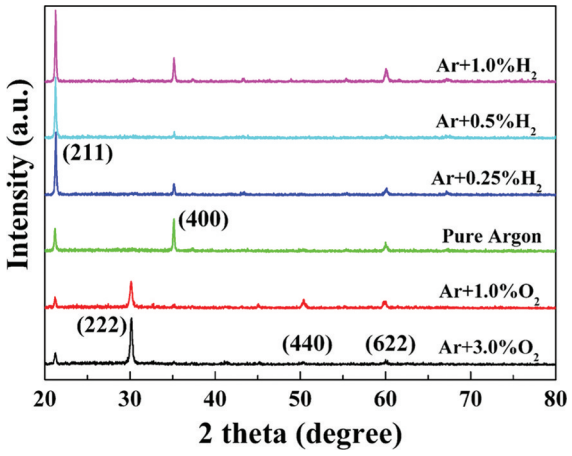

Figure 1. X-ray diffraction patterns of the ITO films deposited with different working atmosphere at the certain sputtering power of 140 W and working pressure of 0.3 Pa.

To further verify the special behavior of the observed (211)-orientation, we examined the ITO films (140 W, 0.3 Pa, 0.5% H_2) by the HRTEM characterization. The grains in Figure 2a are 150-200 nm in size and closely-packed. Figure 2b shows a small area electron diffraction (SAED) pattern. Solid green rings (strong diffractions) and red dotted rings (weak) observed from the as-deposited film match the ideal diffraction pattern of the (211)-oriented In_2O_3 single crystal, as shown in Figure S2 (see the Supporting Information), which further demonstrates the polycrystalline film with the (211)-oriented preference.

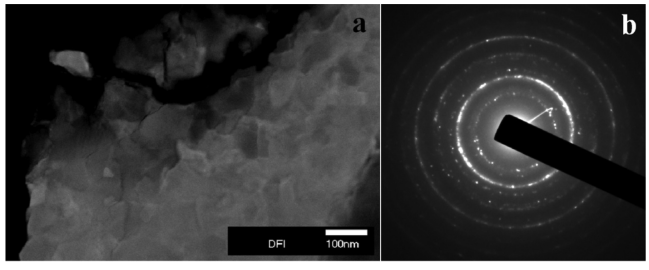

Figure 2. (a) ADF image of ITO films grown at the sputtering power of 140 W and working pressure of 0.3 Pa with Ar/H_2 mixture (0.5% H_2) ambient, (b) related SAED pattern.

3.2. Structural, Electrical, and Optical Properties. Surface and cross-sectional SEM images of three oriented films ((222), (400), (211)), are shown in Figure 3. The surface of the (400)-oriented film consists of 60 nm triangular grains. From the (211)-oriented surface in Figure 3e, the film crystallinity was improved and the grain sizes were enlarged (150-200 nm). The (222)-oriented film is poorer crystallized (Figure 3a), and the grain size is about 10 nm. The films deposited under pure argon and Ar + H_2 tend to form larger

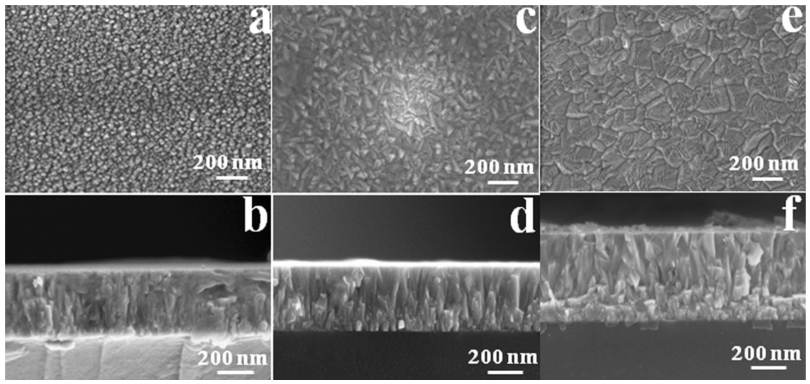

Figure 3. Surface and cross-sectional SEM images of the as-deposited ITO thin films with three typical preferential orientations: (a, b) (222)-oriented, (c, d) (400)-oriented, and (e, f) (211)-oriented, respectively.

grains and a better crystallinity, consistent with the reported result.[23] In an oxygen-deficient especially reduction atmosphere, the growth rate of our films, much faster than that in an O_2 atmosphere results in a stronger orientation preference and larger grain size, which favors transparent conducting properties.

The cross-sectional image of the (211)-oriented film (Figure 3f) reveals larger and more uniform rod-like crystals than the other two (Figure 3b, d). The thickness of the (211) film (490 nm) is significantly larger than the other two, 390 nm for (222) and 430 nm for (400). The respective deposition rates are 13, 14.33, and 16.33 nm/min. It can be noted that the deposition rate of ITO film is the highest in case of weak reducing ambient sputtering. The sufficient energy supply might accelerate crystallization and the crystallization of the sample will be more pronounced by the high deposition rate.

The optical properties of the ITO films ((222), (400), (211)-oriented) are illustrated in Figure 4 and Table 1, and the as-

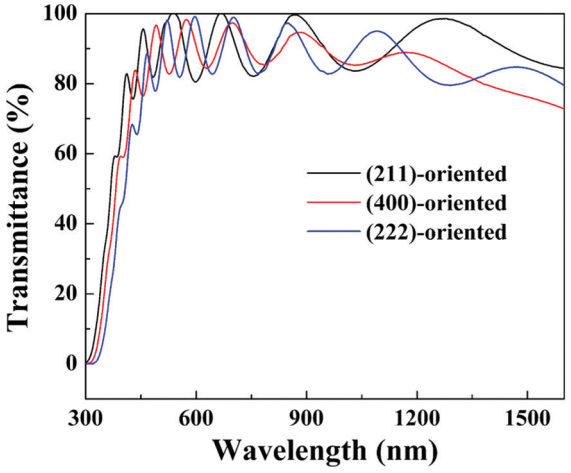

Figure 4. Transmission spectra of ITO films with three typical preferential orientations of (222)-oriented, (400)-oriented, and (211)-oriented, the corresponding thicknesses are 390, 430, and 490 nm, respectively.

sputtered films all exhibit both high visible-light and near-infrared transmittances (>85%). The average transparency of the (211)-oriented film is 89.42% in the range of 400−1100 nm, and the optical band gap (E_g) is 3.80 eV; In comparison, the (222) and (400) films have a lower transmittance (87.24% for (222), 88.25% for (400)) and narrower band gap (3.64 eV for (222), 3.72 eV for (400)), as summarized in Table 1. The maximum band gap of the (211)-oriented film was further evaluated by the band structure simulation below, suggesting the highest conduction band surface. Although the thickness of the (211)-oriented film is larger than the others, its average transmittance is still the highest. The higher transparency of the (211) film below ~400 nm is due to its larger optical band gap, and the higher visible and near-infrared range can be explained by the stronger-aligned orientation and larger grains evidenced by the characterizations of XRD and SEM, which can effectively avoid random light scattering.

The electrical properties of the three films are also studied and compared, as shown in Table 1. Notably, the (211)-oriented film among them exhibits the best conductivity of 1.03×10^{-4} Ω cm and the highest carrier mobility of 30.8 $cm^2/(V\ s)$. The corresponding square resistance reaches as low as 2.11 Ω/sq. The much higher conductivity of the (211)-oriented film than that of (400) and (222) planes must be generated by the richest surface dangling-bonds of In atoms of the plane, which was verified by the surface energy calculation below as the more In-ended surface has a better ability to transfer carriers. The carrier concentrations of the (211) and (400) films (1.95×10^{21} cm^{-3}, 1.89×10^{21} cm^{-3}) are higher than that of the (222) film (0.93×10^{21} cm^{-3}), as listed in Table 1. The (211)-oriented film also exhibits much higher carrier mobility (30.8 $cm^2/(V\ s)$) than the (400) (16.2 $cm^2/(V\ s)$) and (222) (18.3 $cm^2/(V\ s)$) films. The electron mobility is influenced by various factors including the density of scattering centers and crystallographic structure (grain size, grain boundaries, etc.). The higher carrier mobility of the (211) film is related to its microstructure. The film shows a better crystallinity and larger grain size. According to the grain boundary barrier model, the potential barrier existing at the grain boundaries could suppress carrier motion. So the increased Hall mobility might be attributed to the decreasing area of grain boundaries for the increased grain size, which screens the influence of the increased carrier concentration.

3.3. Formation Mechanisms. From the above characterizations and analyses, it can be seen that the different orientations of (222), (400), and (211) ITO films can be prepared by adjusting the sputtering power, working pressure and the atmosphere ambient. In particular, the (211)-oriented films can be precisely formed, and they exhibit much smoother surface and higher conductivity with good transparency. Presumably, the preferential growth control is the most prerequisite for this strict formation.

Table 1. Electrical and Optical Properties of ITO Thin Films with Three Typical Preferential Orientations

preferential orientation	sputtering ambient	thickness (nm)	$R_{\square}$(Ω/sq)	ρ (Ω cm) (×10^{-4})	μ (cm^2/(V s))	T_r (400−1100)	N (cm^{-3}) (×10^{21})	optical E_g (eV)	theoretical E_g (eV)
(222)	Ar + 3%O_2	390	9.44	3.68	18.3	87.24	0.93	3.64	3.08
(400)	Ar	430	4.71	2.02	16.2	88.25	1.89	3.72	2.87
(211)	Ar + 0.5%H_2	490	2.11	1.03	30.8	89.42	1.95	3.80	3.73

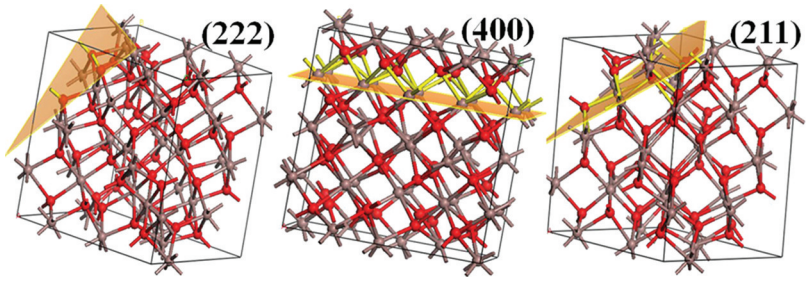

Figure 5. Surface-broken In−O bonds of the cut cell for the (222), (400), and (211) planes by material studio simulation.

The (222), (400), or (211) preferential orientation growth is related to the competition of the corresponding surface energy in the different atmosphere, and this competition has an impact on the modification of the preferential orientation growth from (222) and (400) to (211) in the weak reduction ambient while inversely preferred growth in rich oxidation ambient. Generally, the oxidation of the growing film is in competition with the O_2 removal phenomenon controlled by the RF power density. The low growth rate (high working pressure, low sputtering power, oxygen-rich ambient) allows a more stoichiometric oxide film with the preferential crystallization along (222). The high deposition rate, by increasing RF power or decreasing working pressure especially in the reduction ambient, forms more oxygen-deficient sites to support the (211)-oriented growth.

To explain the special behavior of our samples, the relationship between the preferential orientation and the surface energy of the given crystal plane was investigated. Figure 5 shows the surface state of the cut cell for the (222), (400), and (211) planes, and the surface energy is closely related to the broken bonds on the specific planes. Bond energy is used to estimate the surface energy, as is to say that the surface energy approximately equals to the energy of the bonds broken per unit area

$$E_{surf} = \frac{\sum (n_i E_i)}{2S} \quad (1)$$

Where S is the area of the selected surface, n_i and E_i the number and bond energy of a certain bond in the selected surface.

As for In_2O_3, this formula is simplified as:

$$E_{surf} = \frac{nE_{In-O}}{2S} \quad (2)$$

Where E_{In-O} is 346 kJ/mol. Thus these surfaces were drawn in Figure 5 and the surface energy is estimated by this formula as shown in Table 2.

The calculated surface energy of (222), (400), and (211) planes is 3.890, 6.738, and 9.628 J/m^2, respectively, as shown in Table 2. It can be seen that the (211) orientation not only gives the highest surface energy but has the highest broken bonds per unit cell of 34.3 (13.9 for (222) plane, and 24 for (400) plane), indicating the richest surface dangling-bonds of In atoms for (211) plane. Presumably, magnetron sputtering on the substrate is a thermodynamic unstable process, and the high

Table 2. Surface-Broken Bonds of the Cut Cell for the (222), (400), and (211) Planes and the Calculated Surface Energies by Material Studio Simulation

preferential orientation	broken bonds	cell dimensions (nm^2)	broken bonds per unit cell	surface energy (J/m^2)
(222)	24	$3^{1/2}$	13.9	3.89
(400)	24	1	24	6.74
(211)	21	$6^{1/2}/4$	34.3	9.63

sputtering energy favors forming the comparably higher surface energy plane. The above process can be further assisted by weak reducing ambient because the hydrogen in the atmosphere is inclined to combine with indium and prevent the oxygen from combining. Conclusively, high sputtering power, low working pressure and the weak reducing ambient synergistically result in the formation of the (211)-oriented films.

The band structure of the bixbyite In_2O_3 was calculated by the density function theory. Here, the cutoff energy of plane wave is chosen at 500 eV. For the Brillouin zone (BZ) integration, we use 3 × 3 × 3 Monkhorst−Pack grids. The generalized gradient approximation plus an intra-atomic Coulomb interaction (GGA + U) method was used to open the band gap that is consistent with the experimental value. The Coulombic interaction U and exchange energy J were set to be 8 and 1 eV, respectively.[24] As depicted in Figure 6, the (211) plane has the highest conduction band minimum (CBM) compared with (400) and (222). The calculated theoretical band gap values, as listed in Table 1, indicate that the energy gap of the (211) plane is 3.73 eV, lager than 2.87 eV for (400) and 3.08 eV for (222). The trend fits well with the experimental energy gaps, and the (211) film possesses the widest gap of 3.8 eV (Table 1). The CBM states are mainly composed of In 5s orbitals, and the rich-Indium atom generated highly dispersed In 5s conduction band is favorable to form the highest energy gap at (211) and generate the largest electron mobility (as verified in Table 1).

For (400) and (222) planes, from the point of band gap, the above theoretical prediction is deviated from the experimental results. From Figure 6 it could be seen that the (222) plane has higher CBM than that of (400) plane, whereas the experimental results in Table 1 indicate that the (400) films have wider gap

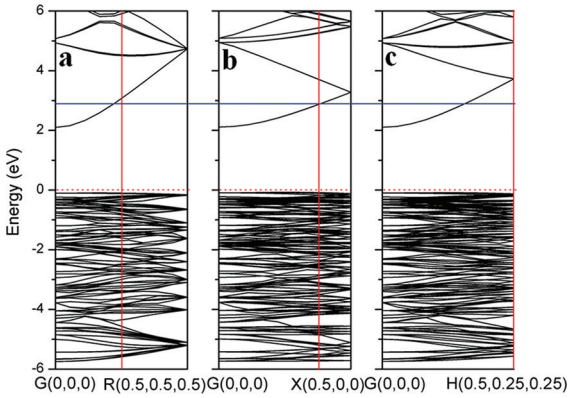

Figure 6. Band structures of (a) (222), (b) (400), and (c) (211) planes in the bixbyite structure of ITO calculated by the density function theory.

of 3.72 eV than that of the (222) films (3.64 eV). The reason might be that the film prepared in pure Argon contains more oxygen vacancies to enhance the carrier concentration (see Table 1) and make the Burstein−Moss effect more notable with larger optical band gap. Here the BM effect contribution for each sample was calculated as a function of the respective carrier concentration basing on the BM equation,[25,26] and the derived band-gap widening caused by the BM shifts are 0.82 eV, 0.80 eV, and 0.50 eV for (211), (400), and (222) films, respectively. The BM effect contributions for (211) and (400) films are much higher than the (222) film and the (211) film is the highest among three, which well-accord to our above results.

4. CONCLUSIONS

In summary, we propose strongly (211)-oriented ITO films to be a very promising transparent electrode, due to the formed high energy gap and generated high conductivity by the rich surface dangling-bonds of In atoms of the plane. The (211)-oriented films can be grown at high sputtering power and low working pressure in the weak reducing ambient. The formation mechanism was studied and the results indicated that the weak reducing ambient favors forming the preferential plane of (211) for the high In-terminated surface state. The superior properties of the (211)-oriented films should be attributed to the comparably highest surface energy and highest conduction band surface comparing with the other two planes of (222) and (400), which was verified by surface energy calculation and band structure simulation. This study not only sheds light on routes to the fabrication of the special (211)-oriented ITO thin films but also discloses insights into the design of the different preferential oriented films in terms of surface modification.

■ ASSOCIATED CONTENT

Ⓢ Supporting Information

A detailed discussion on the effects of the sputtering power and pressure and comparison between our (211)-oriented film and the ideal diffraction pattern of the (211)-oriented In_2O_3 single crystal. This material is available free of charge via the Internet at http://pubs.acs.org/.

■ AUTHOR INFORMATION

Corresponding Author

*E-mail: huangfq@mail.sic.ac.cn (F.H.); liangjun@mail.sic.ac.cn (J.L.).

■ ACKNOWLEDGMENTS

This work is financially supported by National 973 & 863 Program of China Grants 2009CB939903 and 2011AA050505; NSF of China Grants 91122034, 51125006, 51102263, 61076062, and 21101164; NSF of Shanghai Grant11ZR1441900; and Science and Technology Commission of Shanghai Grants 10520706700 and 10JC1415800.

■ REFERENCES

(1) Mutitu, J. G.; Shi, S. Y.; Chen, C. H.; Creazzo, T.; Barnett, A.; Honsberg, C.; Prather, D. W. *Opt. Express* **2008**, *16*, 15238−15248.
(2) Hamberg, I.; Granqivst, C. G. *J. Appl. Phys.* **1986**, *60*, R123−R159.
(3) Wen, S. J.; Counturier, G.; Campet, G.; Portier, J.; Claverier, J. *Phys. Status Solidi A* **1992**, *130*, 407−414.
(4) Park, Y. G.; Seo, K. H.; Lee, J. H.; Kim, J. J.; Cho, S. H.; O'Conner, C. J.; Lee, J. S. *J. Electroceram.* **2004**, *13*, 851−855.
(5) Jung, S.; Park, N. G.; Kwak, M. Y.; Kim, B. O.; Choi, K. H.; Cho, Y. J.; Kim, Y. K.; Kim, Y. S. *Opt. Mater.* **2003**, *21*, 235−241.
(6) Kim, J. H.; Lee, J. H.; Heo, Y. W.; Kim, J. J.; Park, J. O. *J. Electroceram.* **2009**, *23*, 169−174.
(7) Jonda, Ch.; Mayer, A. B. R.; Elschner, U.; Karbach, A. *J. Mater. Sci.* **2000**, *35*, 5645−5651.
(8) Dao, V. A.; Choi, H.; Heo., J.; Park, H.; Yoon, K.; Lee, Y.; Kim, Y.; Lakshminarayan, N.; Yi, J. *Curr. Appl. Phys* **2010**, *10*, 5506−5509.
(9) Das, R.; Adhikary, K.; Ray, S. *Appl. Surf. Sci.* **2007**, *253*, 6068−6073.
(10) Sathiaraj, T. S. *Microelectron. J.* **2008**, *39*, 1444−1451.
(11) Qiao, Z.; Mergel, D. *Thin Solid Films* **2005**, *484*, 146−153.
(12) Terzini, E.; Thilakan, P.; Minarini, C. *Mater. Sci. Eng., B* **2000**, *77*, 110−114.
(13) Wang, S. H.; Zhang, J. Q.; Wang, B.; Feng, L. H.; Cai, Y. P.; Wu, L. L.; Li, W.; Lei, Z.; Li, B. *J. Mater. Sci.: Mater. Electron* **2010**, *21*, 441−444.
(14) Nishimura, E.; Ohkawa, H.; Song, P. K.; Shigesato, Y. *Thin Solid Films* **2003**, *445*, 235−240.
(15) Sasala, R. A.; Sites, J. R. *Sol. Cells* **1991**, *30*, 101−107.
(16) Cui, H. N.; Xi, S. Q. *Thin Solid Films* **1996**, *288*, 325−329.
(17) Vasant Kumar, C. V. R.; Mansingh, A. *J. Appl. Phys.* **1989**, *65*, 1270−1280.
(18) Thilakan, P.; Minarini, C.; Loreti, S.; Terzini, E. *Thin Solid Films* **2001**, *388*, 34−40.
(19) Shigesato, Y.; Paine, D. C. *Thin Solid Films* **1994**, *238*, 44−50.
(20) Ohta, H.; Orita, M.; Hirano, M.; Hosono, H. *J. Appl. Phys.* **2002**, *91*, 3547−3550.
(21) Kim, Y. J.; Jin, S. B.; Kim, S. I.; Choi, Y. S.; Choi, I. S.; Han, J. G. *Thin Solid Films* **2010**, *518*, 6241−6244.
(22) Kumar, K. J.; Raju, N. R. Ch.; Subrahmanyam, A. *Appl. Surf. Sci.* **2011**, *257*, 3075−3080.
(23) Tuna, O.; Selamet, Y.; Aygun, G.; Ozyuzer, L. *J. Phys. D: Appl. Phys.* **2010**, *43*, 055402−7.
(24) Erhart, P.; Klein, A.; Egdell, R. G.; Albe, K. *Phys. Rev. B.* **2007**, *75*, 153205−8.
(25) Jarzebski, Z. M. *Phys. Status Solidi A* **1982**, *71*, 13−41.
(26) Manifacier, J. C.; Szepessy, L.; Bresse, J. F.; Perotin, M.; Stuck, R. *Mater. Res. Bull.* **1979**, *14*, 163−175.